Rare Metal Materials and Engineering
Volume 55, Issue 11, November 2026
Available online at www.rmme.ac.cn

Science Press

Cite this article as: Xie Zheng, Wang Longlong, Tan Chengwen, et al. Process Optimization for Preparing Uniform and Dense Tungsten Coatings on Throat Liners by CVD[J]. Rare Metal Materials and Engineering, 2026, 55(11): 2747-2755. DOI: https://doi.org/10.12442/j.issn.1002-185X.20250595.

ARTICLE

Process Optimization for Preparing Uniform and Dense Tungsten Coatings on Throat Liners by CVD

Xie Zheng[1], Wang Longlong[1], Tan Chengwen[1,2], Yu Xiaodong[1,2], Ning Xianjin[1]

[1] School of Materials Science and Engineering, Beijing Institute of Technology, Beijing 100081, China; [2] Highpure Precision Materials (Suzhou) Co., Ltd, Suzhou 215211, China

Abstract: This study optimized the previously established low-pressure chemical vapor deposition (CVD) model for tungsten, enabling its application under atmospheric pressure conditions to deposit high-performance coatings on the surface of rocket engine throat liners. The effects of three distinct reactor configurations, including a straight-tube inlet, an integrated gas distribution device, and a combination of a distribution device with a flow guide baffle, on the flow dynamics, thermal field, species concentration, and deposition kinetics of reactors were investigated. Numerical and experimental results demonstrate that the configuration incorporating both a distribution device and a baffle eliminates vortices within the liner region by promoting radial gas diffusion, thereby significantly improving flow field uniformity. This optimized design not only improves the uniformity of the deposition rate on the throat insert, but also slightly enhances the service efficiency of tungsten hexafluoride. This work provides a theoretical foundation for designing CVD systems for highly uniform tungsten coatings and offers a practical solution for their engineering application.

Key words: CVD; tungsten; computational fluid dynamics; Fluent

1 Introduction

Tungsten, which possesses the highest melting point (approximately 3410 °C) of all metals, exhibits exceptional physicochemical properties[1–2], including high thermal conductivity of 173 W/(m·K), a low coefficient of thermal expansion, outstanding high-temperature strength, and excellent ablation resistance[3–7]. These characteristics make tungsten highly attractive for rocket applications. Notwithstanding these advantages, its high density (19.35 g/cm^3) and poor machinability severely restrict its direct use[8]. A feasible strategy to circumvent these limitations is the application of tungsten coatings onto lightweight substrates. This approach effectively reduces component density while conferring the superior properties of tungsten to the composite system. Among the techniques for depositing such coatings, physical vapor deposition (PVD), low-pressure chemical vapor deposition (LPCVD), and atmospheric pressure chemical vapor deposition (APCVD) are widely employed[9–13].

Tungsten coatings prepared by PVD are relatively thin, exhibit poor uniformity and inadequate step coverage, and are significantly constrained by the size and shape of the substrate. In addition, the low deposition rate restricts this technique primarily to producing nano- to micro-scale thin films, rendering such coatings unsuitable for harsh service conditions involving high temperature and strong erosion.

In contrast, chemical vapor deposition (CVD) enables the production of tungsten coatings with high purity and density, minimal surface defects, excellent uniformity, and strong adhesion to the substrate, making it well-suited for complex-shaped cavity components. Moreover, compared with LPCVD, APCVD offers a higher deposition rate for tungsten coatings, providing a distinct advantage for the preparation of throat liner coatings[12,14–15].

CVD process is highly controllable, permitting precise adjustment of operational parameters, such as temperature, pressure, and gas flow rate, as well as modification of the reactor geometry to meet diverse application requirements. Extensive research has been devoted to understanding tungsten growth mechanisms in CVD systems. For instance, Bryant[16]

Received date: November 21, 2025
Corresponding author: Tan Chengwen, Ph. D., Professor, School of Materials Science and Engineering, Beijing Institute of Technology, Beijing 100081, P. R. China, E-mail: tanchengwen@bit.edu.cn; Yu Xiaodong, Ph. D., Professor, School of Materials Science and Engineering, Beijing Institute of Technology, Beijing 100081, P. R. China, E-mail: yuxd@bit.edu.cn

Copyright © 2026, Northwest Institute for Nonferrous Metal Research. Published by Science Press. All rights reserved.

determined the activation energy for tungsten deposition via hydrogen reduction of WF_6 to be 67.0 kJ/mol under low-pressure conditions. Subsequently, Pauleau et al[11] established that the deposition rate depends on the partial pressures of the reactants, reporting reaction orders of zero with respect to WF_6 and one-half with respect to H_2 at relatively low pressure. They also correlated the loss of reaction selectivity with an increase in partial pressure of HF. Building on previous research, Lakhotkin et al[17–18] performed a rigorous chemical analysis of the H_2/WF_6 reduction system, concluding that CVD tungsten coating is primarily formed via the disproportionation reaction of tungsten subfluorides (e.g., WF_4).

Numerical simulation has become an indispensable methodology for investigating CVD tungsten coating, complementing experimental studies by enabling the prediction of key parameters such as species concentrations, pressure distribution, and deposition rates within the reactor. The foundation for such modeling was established by Arora et al[[19], who developed a detailed mechanistic framework for the H_2 reduction of WF_6 using statistical mechanics and transition state theory. Building on this, Kleijn et al[20] refined this model and implemented it within the PHOENICS computational fluid dynamics (CFD) software, facilitating the optimization of thin-film deposition processes. Raumann et al[21–23] developed a model for tungsten-fiber-reinforced tungsten (W_f/W) composites and used this model to propose new deposition rate equations. These equations allow the calculation of partial pressures in CVD reactors and facilitate the modeling of reactions for W_f/W composites, thus enabling the prediction of interfacial contact conditions and potential pore formation on tungsten substrates. Using their CFD-optimized process parameters, dense W_f/W composites at a H_2: WF_6 flow ratio of 12.5: 1 were synthesized. Furthermore, they simulated tungsten synthesis using the commercial software COMSOL Multiphysics and experimentally validated the accuracy of the model. Raumann et al[21–23] also investigated the dependence of the deposition rate on the partial pressure of WF_6, ultimately proposing a new rate equation that incorporates modified semi-empirical constants. Wang et al[24] used ANSYS Fluent to simulate CVD tungsten deposition process and adopted an orthogonal experimental design to optimize process parameters, thereby identifying the optimal parameter combination for simultaneously maximizing the deposition rate and coating uniformity.

Although extensive research has been conducted on tungsten deposition via CVD, the vast majority of existing studies focused on elucidating the fundamental reaction mechanisms of CVD tungsten coating and formulating empirical deposition rate equations. However, systematic investigations into the structural optimization of CVD reactors tailored specifically for complex-shaped components remain scarce. Achieving a uniform, dense tungsten coating on rocket engine throat liners—a typical representative of such complex-shaped hot-end components—remains a significant technical challenge, as their intricate profiled geometry induces severe local inhomogeneities in gas flow distribution, thermal field, and reactant diffusion paths at the substrate surface. This imposes stringent requirements for the precise regulation of gas-phase parameters (e. g., precursor concentration, flow velocity, and pressure distribution) at the coating-substrate interface, which is essential to avoid critical coating defects, including non-uniform thickness, poor compactness, and low deposition efficiency. Notably, the coupling effects of reactor structure on the flow field, thermal field, and precursor concentration field, which are the core factors governing coating uniformity for irregular substrates, have not been fully explored or quantitatively characterized to date. To address this critical research gap and overcome the corresponding engineering bottleneck, this study innovatively employed CFD to conduct a coupled multi-physical field analysis, integrating flow field, thermal field, species concentration field, and deposition kinetics, for an APCVD reactor dedicated to rocket engine throat liners. Three distinct reactor inlet configurations were systematically investigated and optimized, and the reliability of the numerical simulation results was validated through controlled deposition experiments. For experimental validation, high-purity tungsten hexafluoride (WF_6, 99.999vol%) and hydrogen (H_2, 99.999vol%) were used as precursor gases to prepare high-performance tungsten coatings on throat liner substrates under atmospheric pressure conditions, with the ultimate objective of developing a structurally optimized APCVD reactor that enables the deposition of uniform, dense tungsten coatings on complex-shaped aerospace components.

2 Numerical Simulation and Experiment

2.1 Numerical simulation method

The deposition process via the hydrogen reduction of WF_6 can be divided into three consecutive kinetic stages: (1) mass transport: it involves the diffusion of H_2 and WF_6 toward the substrate surface and the escape of HF from the reaction zone, and its rate is predominantly determined by hydrodynamic parameters (e.g., Reynolds number and Schmidt number); (2) boundary layer diffusion: it involves the transfer of reactants (H_2 and WF_6) and products (tungsten and HF) across the boundary layer; (3) surface reaction: it contains the adsorption of reactant molecules on the substrate surface, heterogeneous surface chemical reactions, and the desorption of reaction products, and its rate is governed by surface chemical kinetics.

To simplify the numerical model, the following assumptions are adopted for the deposition process: (1) the deposition process is approximated as a single-step reaction; (2) the effect of substrate surface roughness on boundary-layer mass transfer is neglected; (3) the kinetic effects related to surface adsorption and desorption processes are neglected. Although these simplifying assumptions may compromise the model accuracy, they significantly enhance computational efficiency while preserving the key features of the main physical phenomena.

2.1.1 Geometric model and mesh generation

To improve process efficiency and the utilization rate of

WF_6, this study deposits tungsten coatings on two liners simultaneously, laying the foundation for large-scale coating deposition on multiple liners.

CVD reactor system for tungsten coating preparation mainly contains a gas inlet device and a cylindrical reaction chamber, where the main deposition reactions occur. Fig. 1 shows the schematic diagrams of the deposition chamber structures. Fig. 1e and 1f show three-dimensional structural diagrams of the gas distribution device and the flow baffle, respectively. Previous research results have shown that the gas distribution device can improve the gas flow distribution in the reaction chamber, which mainly achieves its function by dispersing a single large gas flow into multiple small gas flows. The flow baffle can guide the gas flow along the wall surface, avoiding the occurrence of eddy currents in the gas flow in the deposition chamber.

To optimize computational accuracy and efficiency, a differentiated mesh generation strategy is used for different regions: hexahedral meshes are applied to the upper and lower flow field regions of the throat liner, while locally refined tetrahedral meshes are used for the complex structural areas of the reaction chamber adjacent to the throat liner. Additionally, boundary layers are incorporated in the region near the throat liner wall to ensure the accuracy of computational results. Fig.2 shows the mesh generation of the deposition chamber.

2.1.2 Boundary conditions

The boundary conditions considered in this study include flow velocity, pressure, temperature, and heat transfer coefficient at the inlet, outlet, and various wall surfaces (i.e., interfaces involving mass and energy exchange). These boundary conditions are determined using historical empirical values and calculations based on the corresponding specific experimental parameters. The flow rate of H_2 is 2.2 L/min, and that of WF_6 is 10 g/min. The heating temperature is 560 °C (833 K).

2.2 Experimental methodology

Fig. 3 shows the schematic diagram of the experimental setup for CVD of tungsten. The deposition process was conducted at a pressure slightly above atmospheric pressure to prevent air ingress, which would oxidize contaminants and compromise coating quality. Mass flow meters provided precise regulation of the gas flow rates. The outlet of the deposition chamber was connected to a tail gas treatment system, where reaction by-products, such as HF, were neutralized by a saturated $Ca(OH)_2$ solution, enabling the safe disposal of the tail gas.

3 Results and Discussion

3.1 Influence of different structures on gas velocity field

Owing to its axisymmetric geometry, the two-dimensional cross-sectional condition of the deposition chamber can be observed to analyze the entire chamber. Fig. 4 presents the simulated velocity distributions for the three reactor configurations. In all cases, the constricted geometry of the throat liner induces a pronounced flow acceleration, as evidenced by the increased velocity within the liner section.

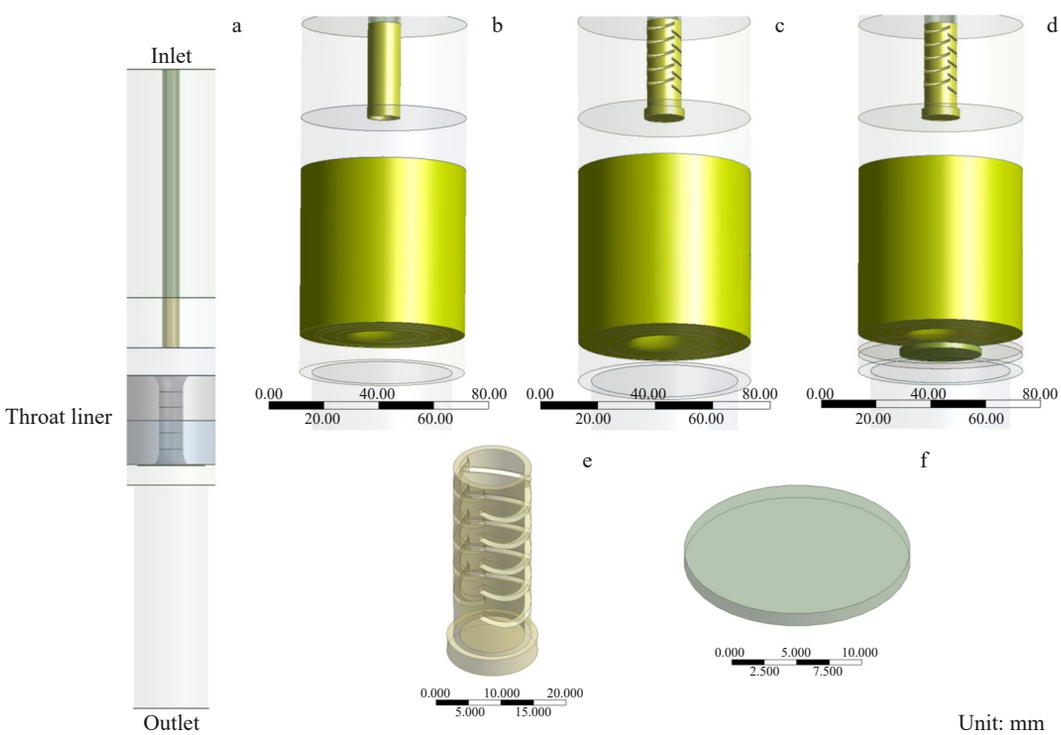


Fig.1 Schematic diagrams of the deposition chamber structures: (a) deposition chamber with a straight-tube gas inlet; (b) key part of the deposition chamber with a straight-tube gas inlet; (c) key part of the deposition chamber with a gas distribution device; (d) key part of the deposition chamber with both a gas distribution device and a flow baffle; (e) three-dimensional structure of the gas distribution device; (f) three-dimensional structure of the flow baffle

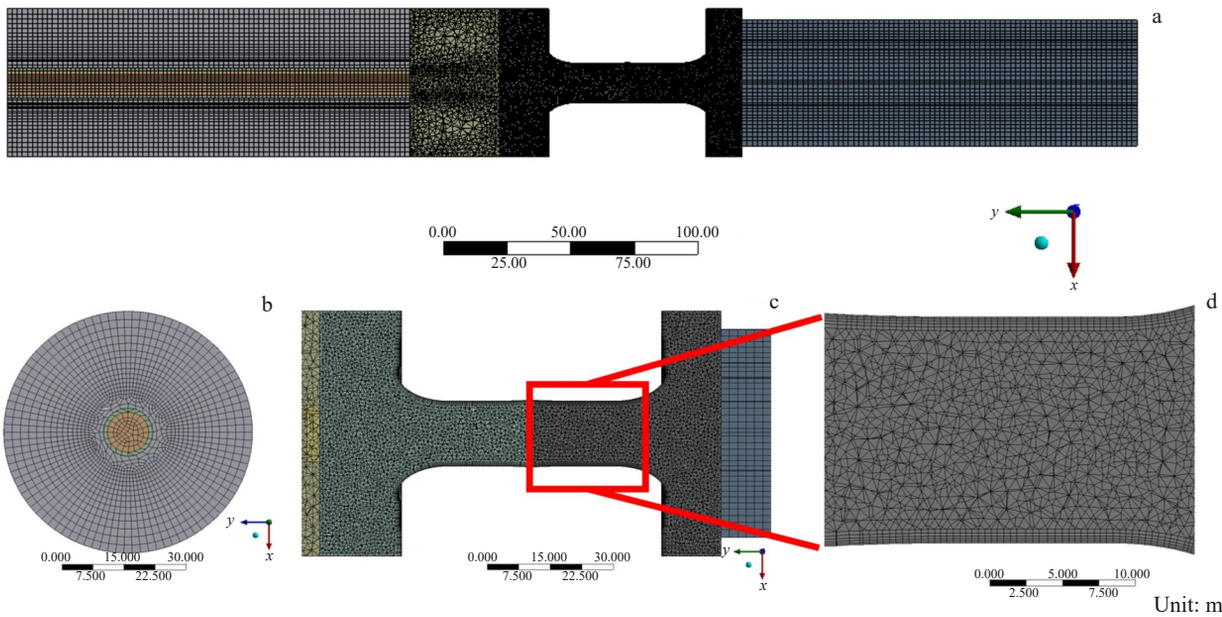


Fig.2 Mesh generation of the deposition chamber: (a) cross-sectional mesh on the *x*-*y* plane; (b) mesh along the *y* direction; (c) mesh near the throat liner; (d) mesh of a partial region of the throat liner

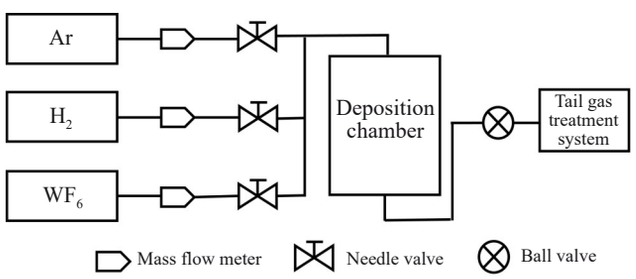


Fig.3 Schematic diagram of the experimental setup for CVD tungsten coating deposition

In the straight-tube inlet configuration (Fig. 4a), the main gas flow is directed axially into the liner cavity, resulting in significant velocity inhomogeneity above the throat liner. Analysis of the local flow field reveals that the contoured geometry of the liner induces localized vortices near the inlet, which disrupt the uniform distribution of reactants. The integration of a gas distribution device (Fig.4b) addresses this issue by altering the gas introduction to a gradual lateral flow. This mode prevents direct impingement, promotes controlled gas accumulation above the liner, and effectively suppresses vortex formation. However, in this configuration, gas exiting the liner cavity flows directly downward, depleting the reactant concentration at the trailing end of the throat liner and adversely affecting the reaction kinetics. This restriction is mitigated by the addition of a flow baffle (Fig. 4c). In this

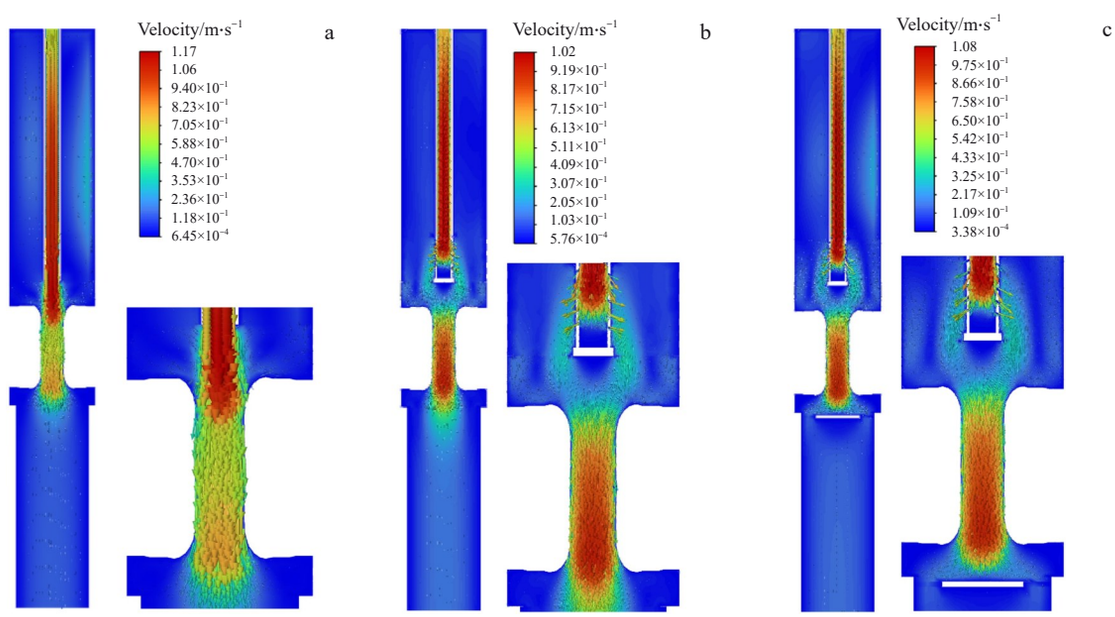


Fig.4 Velocity contour plots of three reactor configurations: (a) straight-tube inlet deposition chamber; (b) deposition chamber with a gas distribution device; (c) deposition chamber with both a gas distribution device and a flow baffle

optimized design, the gas exiting the liner is redirected radially outward, maintaining higher reactant concentrations in the bilateral regions and thereby promoting a uniform tungsten deposition rate across the entire liner surface. The resulting stable and uniform flow distribution significantly enhances deposition efficiency and coating quality, ultimately yielding a more uniform and denser tungsten coating.

3.2 Influence of different structures on temperature field

Fig. 5 presents the temperature distributions for the three reactor configurations. Analysis indicates a uniform surface temperature within the liner cavity across all three configurations. The temperature in the upper fluid region and along the cold walls progressively decreases from the central heating zone toward the chamber ends. In contrast, the lower fluid region maintains a stable thermal profile. This stability is attributed to the fact that the gas leaving the liner cavity is sufficiently heated to 800 K, resulting in a minimized thermal gradient in the lower chamber section.

In the straight-tube configuration (Fig. 5a), the straight-tube gas inlet causes the reactive gases not to be sufficiently preheated, leading to a decrease in internal temperature of the throat liner. This suboptimal temperature can hinder the kinetics of the tungsten deposition reaction, ultimately compromising coating quality. In contrast, the configurations employing gas distribution devices (Fig. 5b–5c) alter the gas inlet methodology, allowing for sufficient preheating of the reactant gases prior to their entry into the liner. This enhanced thermal homogenization elevates the cavity temperature to near-optimal levels, thereby improving deposition efficiency and yielding tungsten coatings with superior uniformity and density.

3.3 Influence of different structures on gas concentration field

Fig. 6 and Fig. 7 present the mole fraction distributions of H_2 and WF_6, respectively, for the three chamber configurations. A comparative analysis reveals that the distinct structural designs significantly influence the concentration profiles of both precursor gases.

In the straight-tube configuration (Fig. 6a), the direct injection of gas into the liner cavity, coupled with vortex formation above it, results in a significantly higher mole fraction of hydrogen inside the inlet tube than that in the surrounding region. This pronounced inhomogeneity adversely affects the uniformity of CVD reaction rate. As shown in Fig. 6b and 6c, the incorporation of a gas distribution device shifts the inlet mode from axial to lateral introduction. This change enhances the uniformity of the hydrogen distribution and suppresses vortex formation. However, in the configuration with only the distribution device (Fig. 6b), the downward flow of gas exiting the liner cavity depletes the mole fraction of hydrogen near the base, consequently reducing the local deposition rate. This limitation is resolved in the final configuration (Fig. 6c), where a flow baffle redirects the effluent gas laterally. This prevents the depletion of hydrogen at the liner base, ensuring a more consistent reactant concentration and deposition rate.

The content (mole fraction) distribution of the primary reactant, WF_6, generally correlates with that of H_2. Given the high cost of WF_6, its utilization efficiency is a critical metric for reactor performance. Across all configurations, the WF_6 content is the highest at the inlet and decreases toward the outlet. In both the straight-tube and the gas distribution device configurations (Fig. 7a–7b), the WF_6 concentration decreases from approximately 25mol% at the inlet to 15mol% at the exhaust. In the optimized configuration featuring both a distribution device and a flow baffle (Fig. 7c), the inlet concentration remains at 25mol%, while the outlet concentration drops further to 12mol% . This significantly lower outlet concentration demonstrates a more complete consumption of the precursor, confirming a higher WF_6 utilization efficiency

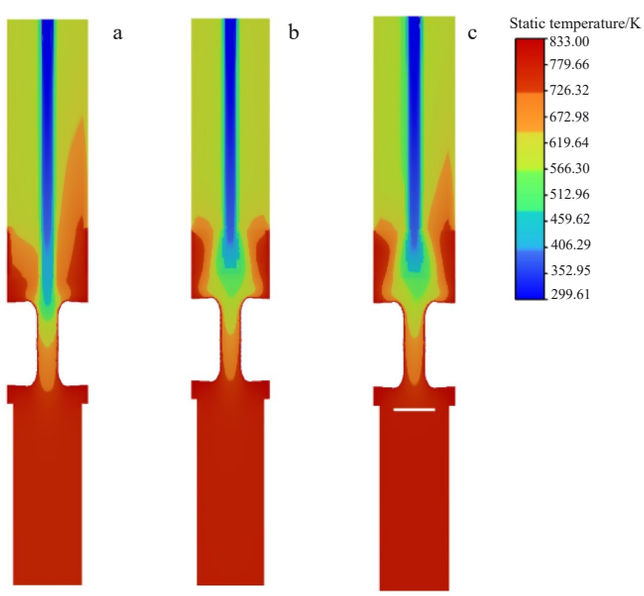


Fig.5 Temperature contour plots of three reactor configurations: (a) straight-tube inlet deposition chamber; (b) deposition chamber with a gas distribution device; (c) deposition chamber with both a gas distribution device and a flow baffle

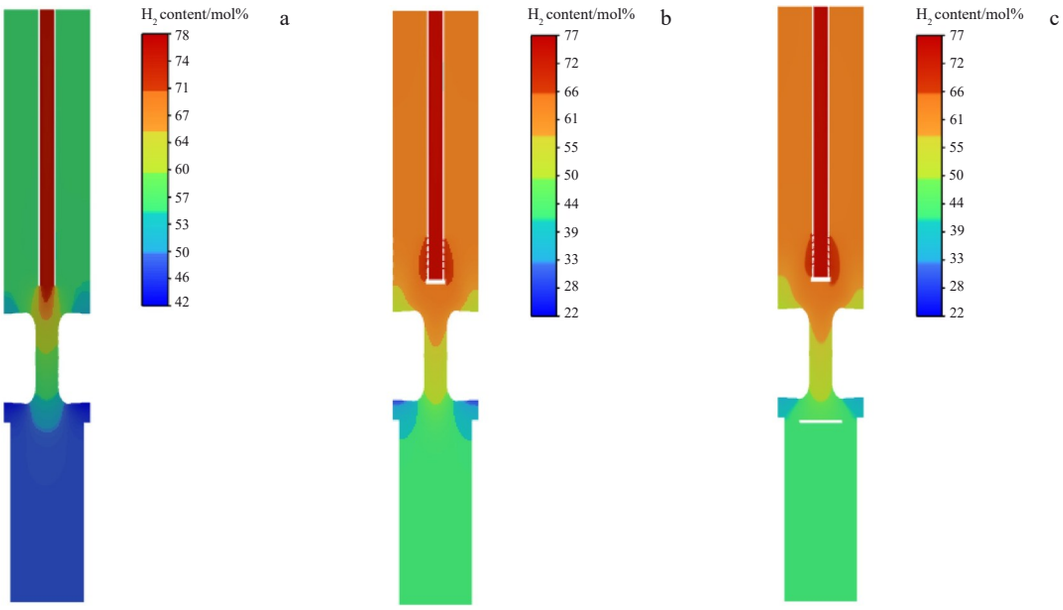


Fig.6 Contour plots of H_2 content distribution in deposition chambers with different structures: (a) straight-tube inlet deposition chamber; (b) deposition chamber with a gas distribution device; (c) deposition chamber with both a gas distribution device and a flow baffle

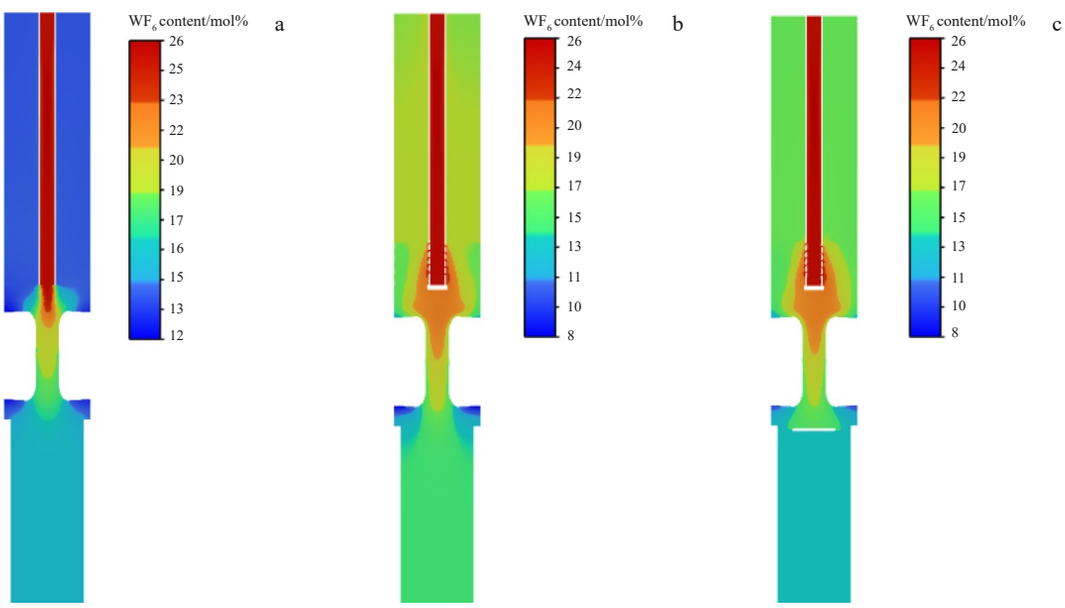


Fig.7 Contour plots of WF_6 content distribution in deposition chambers with different structures: (a) straight-tube inlet deposition chamber; (b) deposition chamber with a gas distribution device; (c) deposition chamber with both a gas distribution device and a flow baffle

in the final design.

3.4 Distribution of tungsten deposition rate on throat liner surface

Fig.8 presents the tungsten deposition rate profiles along the throat liner cross-section for the three reactor configurations, with the positive *x*-axis corresponding to the gas flow direction. The deposition rate in the straight-tube inlet chamber is markedly lower than that in the configurations employing gas distribution devices. This is attributed to insufficient preheating of the reaction gases in the straight-tube design, which results in a lower substrate temperature and consequently suppresses the deposition reaction kinetics.

In the upstream region, the deposition rates for chambers

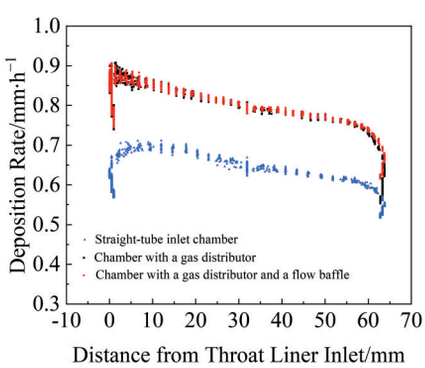


Fig.8 Simulated tungsten deposition rates on throat liner surface of three different deposition chambers

with a gas distribution device (either with or without a baffle) are comparable. A significant divergence, however, occurs downstream, where the configuration incorporating the flow baffle exhibits a markedly higher deposition rate. This demonstrates that the combination of a gas distribution device and a flow baffle can enhance process homogeneity by improving the distribution of reactant gases and the thermal profile within the liner cavity.

3.5 Verification experiment

To validate the simulation results, tungsten coatings were deposited using the two highest-performing reactor configurations identified by CFD analysis: one with the gas distribution device and the other incorporating both a distribution device and a flow baffle. Fig. 9 shows the actual deposition reaction chamber. Fig. 9a presents the assembled experimental apparatus, including the heating system, gas inlet system, reaction chamber, and other components. Fig. 9b shows the reaction chamber equipped with thermocouples for temperature measurement. Fig. 9c and 9d display photographs of the gas distribution device and the flow baffle, respectively. This deposition device can operate stably for more than 48 h.

Fig. 10 presents a comparative analysis of the simulated and experimentally measured deposition rates, alongside cross-sectional morphologies of the tungsten coatings, for the reactor configurations with a gas distribution device and with both a device and a flow baffle. In the current study, the simulated deposition rates consistently overestimate the experimental measurements. This deviation arises from the fact that in the simulation of the deposition experiment, CVD reaction was only applied on the inner surface of the throat liner. In actual deposition, however, deposition reactions also occur on the walls of the cylindrical reaction chamber, the gas distribution device, and other surfaces. Compared with the simulated deposition reactions, these actual reactions consume the reactants in advance, resulting in a higher simulated deposition rate. To align the model with empirical data, the simulated rates were adjusted using a correction factor of 0.8. The coatings exhibit uniform adhesion to the carbon-carbon (C/C) substrate, and are macroscopically defect-free, without pores, cracks, or protrusions. In the range of 0–50 mm, the deposition rates in both reaction chambers are approximately 0.6 mm/h. This is in good agreement with the revised simulated deposition rate. Critically, the experimental data confirm the simulated trend: the deposition rate decreases along the contour of the throat liner in the flow direction. As can be seen from Fig. 10, after installing the flow baffle, the tungsten deposition rate is significantly improved in the region beyond 50 mm. Specifically, it increases from the original 0.40 mm/h to 0.50 mm/h at 55 mm. And at 60 mm, the tungsten deposition rate is raised from approximately 0 mm/h to 0.3 mm/h. Critically, the experimental data confirm the simulated trend that the deposition rate decreases along the contour of the throat liner in the flow direction. The magnitude of this decrease is significantly reduced in the configuration incorporating the flow baffle. This result validates that the flow baffle effectively mitigates the downstream depletion of reactants, leading to a more uniform deposition profile.

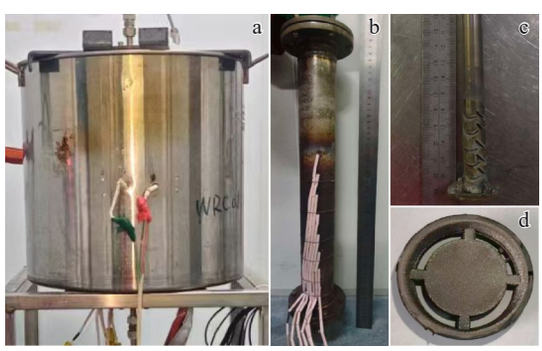


Fig.9 Appearances of deposition reaction chamber: (a) assembled experimental apparatus; (b) reaction chamber equipped with thermocouples; (c) gas distribution device; (d) flow baffle

The deviation between simulated and experimental deposition rates in the lower liner region is attributed to a phenomenon not included in CFD model: deposition of tungsten on the flow baffle itself. This competing reaction consumes reactant species, reducing the concentration of reactant gas at the substrate surface and leading to the observed suppression of the local deposition rate.

Fig. 11 presents metallographic micrographs of the resulting CVD tungsten coatings, showing the microstructures at the outlet region and a planar surface region of the throat liner.

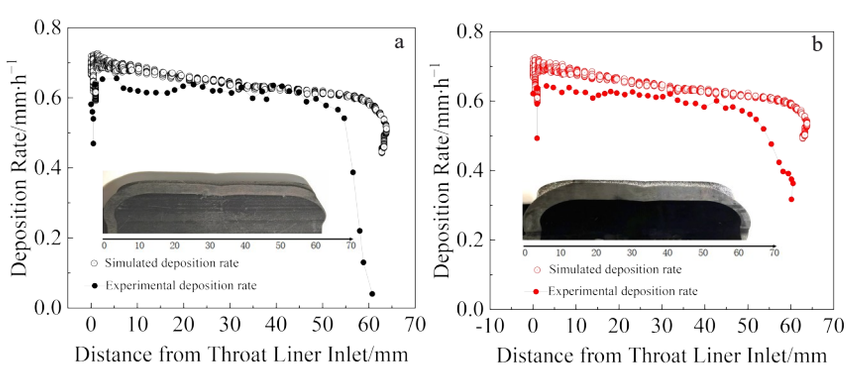


Fig.10 Comparison of experimental and simulated deposition rates and appearances of physical tungsten coating samples in two deposition chambers: (a) chamber with a gas distribution device; (b) chamber with both a gas distribution device and a flow baffle

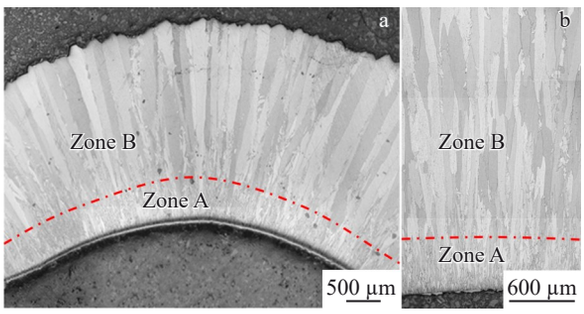


Fig.11 Metallographic microstructures of CVD tungsten coating at outlet region (a) and planar surface region (b) of the throat liner

The deposited tungsten exhibits a polycrystalline microstructure, growing primarily in the direction normal to the substrate surface. The coating morphology can be delineated into two distinct zones along the growth direction. Zone A (competitive growth zone), which is located adjacent to the substrate, is characterized by initial nucleation and competitive growth. The gradual increase in grain width indicates a growth competition, where preferentially oriented grains outcompete and eliminate their neighbors. Zone B is columnar grain zone. In this upper region, competitive growth ceases. The grains exhibit a stable, columnar morphology with minimal width variation, indicating a transition to self-similar growth, where the dominant crystal orientations have prevailed.

The density of the tungsten coating was measured using the Archimedes displacement method, and it reaches 19.17 g/cm^3, which is close to the theoretical density of tungsten (19.35 g/cm^3). Fig. 12 shows the morphologies of the top surface and cross-section of CVD tungsten coating. As can be seen from Fig. 12a, the surface of the tungsten coating is composed of numerous “pyramids”, which represent the outermost exposed tops of CVD tungsten grains. Fig. 12b indicates that CVD coating is dense and essentially free of internal defects. As illustrated in Fig. 12c, the deposited tungsten fills the pores of the substrate and forms an anchoring bond with the substrate.

To characterize the bonding strength between the tungsten coating and C/C substrate, cylindrical samples with a diameter

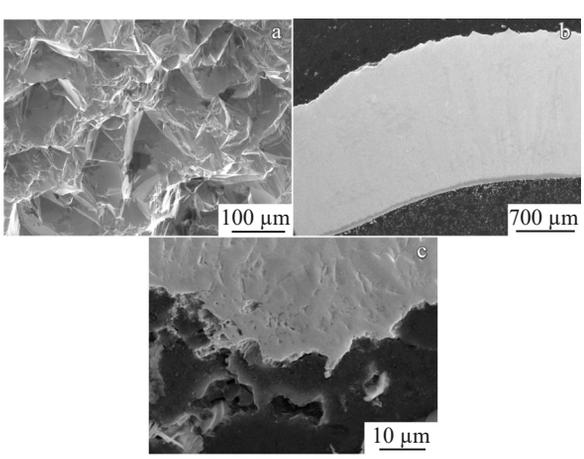


Fig.12 Morphologies of CVD tungsten coating: (a) top surface; (b) cross-section; (c) interface between tungsten coating and substrate

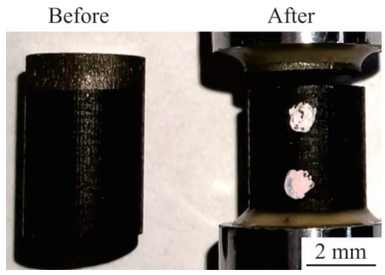


Fig.13 Photographs of the samples before and after tensile test

of 8 mm were cut from the throat liner for tensile testing. Fig. 13 shows the photographs of the samples before and after the tensile test. A large number of substrate carbon particles and carbon fibers adhere to the fracture surface, indicating that excellent bonding between the coating and the substrate has been achieved. The fracture occurs mainly inside the substrate. In fact, since C/C composite is a porous material with multi-scale interfaces inside, the bonding strength between these internal interfaces is lower than that between the coating and the substrate. Consequently, the failure during tensile testing is initiated preferentially within the substrate. The results show that the tensile strength between the coating and the substrate is approximately 4.6 MPa.

4 Conclusions

1) CVD reactor for depositing tungsten coatings on rocket engine throat liners was optimized by integrating CFD simulation with experimental validation.

2) A straight-tube inlet configuration generates vortices above the liner, resulting in non-uniform temperature and reactant concentration fields. Replacing this with a lateral gas distribution device enhances flow distribution and gas preheating, mitigating temperature gradients; however, it fails to prevent a significant downstream decrease in deposition rate.

3) The optimized design—incorporating both a gas distribution device and a flow baffle—successfully eliminates vortices by promoting radial flow diffusion. This creates a uniform flow field and stable thermal environment, which ensures consistent reaction conditions. Finally, the tungsten coating exhibits a density of 19.17 g/cm^3, and bonds well with the substrate.

4) By adapting a LPCVD model for atmospheric-pressure operation, this work has successfully addressed the critical challenge of depositing uniform, high-quality tungsten coatings on complex-shaped components. The optimization strategy and validated model presented in this research provide a robust framework for the design of high-performance CVD systems for advanced aerospace applications.

References

1 Donchev A, Mengis L, Couret A *et al. Intermetallics*[J], 2021, 139: 107270

2 Zhang Shihui, Wang Kaijun, Hu Jin *et al. Rare Metal Materials*

and Engineering[J], 2021, 50(11): 4073 (in Chinese)
3 Popov O, Vishnyakov V. *Journal of Nuclear Materials*[J], 2025, 611: 155817
4 Weerasinghe A, Wirth B D, Maroudas D. *Journal of Applied Physics*[J], 2022, 132(18): 185102
5 Škoro G P, Bennett J R J, Edgecock T R *et al. Journal of Nuclear Materials*[J], 2012, 426(1): 45
6 Lee D, Umer M A, Ryu H J *et al. International Journal of Refractory Metals and Hard Materials*[J], 2014, 43: 89
7 Greuner H, Bolt H, Böswirth B *et al. Fusion Engineering and Design*[J], 2005, 75–79: 333
8 Zhan J L, Wang H L, Wang H L *et al. International Journal of Refractory Metals and Hard Materials*[J], 2024, 123: 106773
9 Quesnel E, Pauleau Y, Monge-Cadet P *et al. Surface and Coatings Technology*[J], 1993, 62(1): 474
10 Lian Y Y, Liu X, Cheng Z K *et al. Journal of Nuclear Materials*[J], 2014, 455(1): 371
11 Pauleau Y, Lami P. *Journal of the Electrochemical Society*[J], 1985, 132(11): 2779
12 Lv Y W, Song J P, Lian Y Y *et al. Journal of Nuclear Materials*[J], 2015, 457: 317
13 Zhang M, Hu C Y, Cai H Z *et al. Rare Metal Materials and Engineering*[J], 2022, 51(8): 2830
14 Zhou Z, Tao C F, Chen B *et al. Advanced Engineering Materials*[J], 2023, 25(12): 2201781
15 Lian Y Y, Feng F, Wang J B *et al. Journal of Nuclear Materials*[J], 2019, 513: 241
16 Bryant W A. *Journal of the Electrochemical Society*[J], 1978, 125(9): 1534
17 Lakhotkin Y V. *Protection of Metals*[J], 2008, 44(4): 319
18 Lakhotkin Y V, Kuz'min V P, Rybkina T I *et al. Inorganic Materials*[J], 2000, 36(5): 454
19 Arora R, Pollard R. *Journal of the Electrochemical Society*[J], 1991, 138(5): 1523
20 Kleijn C R, Dorsman R, Kuijlaars K J *et al. Journal of Crystal Growth*[J], 2007, 303(1): 362
21 Raumann L, Coenen J W, Riesch J *et al. Surface and Coatings Technology*[J], 2020, 381: 124745
22 Raumann L, Coenen J W, Riesch J *et al. Metals*[J], 2021, 11(7): 1089
23 Raumann L, Coenen J W, Riesch J *et al. Nuclear Materials and Energy*[J], 2021, 28: 101048
24 Wang Y F, Peng L P, Zhao Y D *et al. ACS Omega*[J], 2025, 10(18): 18571

CVD法在喉衬上制备均匀致密钨涂层的工艺优化

谢　铮[1]，汪龙龙[1]，谭成文[1,2]，于晓东[1,2]，宁先进[1]
(1. 北京理工大学 材料学院，北京 100081)
(2. 海朴精密材料（苏州）有限责任公司，江苏 苏州 215211)

摘　要：本研究对已建立的钨低压化学气相沉积（CVD）模型进行改进，使其可在常压条件下于火箭发动机喉衬表面沉积高性能涂层。研究分析了三种不同反应器结构（直管进气反应室、加装布气装置反应室、加装布气装置与引流板反应室）以及结构对反应室内流动特性、温度场、组分浓度及沉积反应的影响。数值模拟与实验结果表明，采用布气装置与引流板相结合的反应室可通过增强气体径向扩散，消除反应室喉衬处的涡流，从而显著提升流场均匀性。该优化设计不仅提高了喉衬构件表面沉积速率的均匀性，还小幅提升了六氟化钨的利用效率。本研究为高均匀性钨涂层CVD系统的设计提供了理论基础，同时为其工程化应用提供了可行方案。

关键词：CVD；钨；计算流体力学；Fluent

作者简介：谢 铮，男，2002年生，硕士生，北京理工大学材料学院，北京 100081，E-mail：3120231005@bit.edu.cn